AGU PUBLICATIONS

Journal of Advances in Modeling Earth Systems

RESEARCH ARTICLE

10.1002/2015MS000463

Key Points:
- We compare a family of functionally similar biogeochemical models with 3, 6, and 30 tracers
- Nutrient and gas simulations are similar across all three, under both preindustrial and rising CO_2
- Reduced-tracer models can provide low-cost yet complex biogeochemical simulations at high resolution

Supporting Information:
- Supporting Information S1
- Software S1

Correspondence to:
E. Galbraith,
eric.d.galbraith@gmail.com

Citation:
Galbraith, E. D., et al. (2015), Complex functionality with minimal computation: Promise and pitfalls of reduced-tracer ocean biogeochemistry models, *J. Adv. Model. Earth Syst.*, *7*, 2012–2028, doi:10.1002/2015MS000463.

Received 3 APR 2015
Accepted 17 NOV 2015
Accepted article online
Published online 21 DEC 2015

Complex functionality with minimal computation: Promise and pitfalls of reduced-tracer ocean biogeochemistry models

Eric D. Galbraith[1,2], John P. Dunne[3], Anand Gnanadesikan[4], Richard D. Slater[5], Jorge L. Sarmiento[5], Carolina O. Dufour[5], Gregory F. de Souza[5], Daniele Bianchi[2,7], Mariona Claret[2], Keith B. Rodgers[5], and Seyedehsafoura Sedigh Marvasti[4,6]

[1]Institucio Catalana de Recerca i Estudis Avancats—Institut de Ciencia i Tecnologia Ambientals, Universitat Autonoma de Barcelona, Bellaterra, Barcelona, Spain, [2]Department of Earth and Planetary Science, McGill University, Montreal, Québec, Canada, [3]NOAA Geophysical Fluid Dynamics Laboratory, Princeton New Jersey, USA, [4]Department of Earth and Planetary Sciences, Johns Hopkins University, Baltimore, Maryland, USA, [5]Atmospheric and Oceanic Science Program, Princeton University, Princeton, New Jersey, USA, [6]Department of Marine Sciences, Science and Research Branch, Islamic Azad University, Tehran, Iran, [7]Department of Atmospheric and Oceanic Sciences, University of California, Los Angeles, CA, USA

Abstract Earth System Models increasingly include ocean biogeochemistry models in order to predict changes in ocean carbon storage, hypoxia, and biological productivity under climate change. However, state-of-the-art ocean biogeochemical models include many advected tracers, that significantly increase the computational resources required, forcing a trade-off with spatial resolution. Here, we compare a state-of-the art model with 30 prognostic tracers (TOPAZ) with two reduced-tracer models, one with 6 tracers (BLING), and the other with 3 tracers (miniBLING). The reduced-tracer models employ parameterized, implicit biological functions, which nonetheless capture many of the most important processes resolved by TOPAZ. All three are embedded in the same coupled climate model. Despite the large difference in tracer number, the absence of tracers for living organic matter is shown to have a minimal impact on the transport of nutrient elements, and the three models produce similar mean annual preindustrial distributions of macronutrients, oxygen, and carbon. Significant differences do exist among the models, in particular the seasonal cycle of biomass and export production, but it does not appear that these are necessary consequences of the reduced tracer number. With increasing CO_2, changes in dissolved oxygen and anthropogenic carbon uptake are very similar across the different models. Thus, while the reduced-tracer models do not explicitly resolve the diversity and internal dynamics of marine ecosystems, we demonstrate that such models are applicable to a broad suite of major biogeochemical concerns, including anthropogenic change. These results are very promising for the further development and application of reduced-tracer biogeochemical models that incorporate "sub-ecosystem-scale" parameterizations.

1. Introduction

In recent years, the numerical models used to evaluate climate change have begun to incorporate representations of ocean biogeochemical cycling. This is motivated by a number of goals, of which four are highlighted here:

1. Climate models are increasingly being asked to predict future climate given human emissions of carbon dioxide. The ocean represents a reservoir of carbon that is a factor of ≈40 larger than the atmospheric reservoir [*Siegenthaler and Sarmiento*, 1993] and ocean biology accounts for a significant fraction of this storage [*Marinov et al*., 2008]. Today, the ocean takes up approximately one quarter of the carbon added to the atmosphere by human activity [*Wanninkhof et al*., 2013], reducing the impact of anthropogenic carbon emissions on climate. Changes in the oceanic storage of carbon dioxide have been invoked to explain much of the 80 ppmv difference in atmospheric carbon dioxide between the last glacial maximum and preindustrial atmosphere [*Sigman and Boyle*, 2000], implying a significant climate sensitivity of the oceanic carbon sink. Insofar as a sensitivity of this type may be expressed under climate change, changes in ocean biogeochemistry could substantially alter the future trajectory of atmospheric carbon dioxide.

2. The dissolution of carbon dioxide in seawater produces carbonic acid. As a result, the oceanic uptake of carbon dioxide leads to an inexorable acidification of seawater [*Orr et al*., 2005; *Doney et al*., 2009]. Although the impacts of acidification on marine organisms are poorly known, there is great concern that calcifying organisms and larval fish may be affected in complex ways should pH continue to fall [*Kroeker et al*., 2013]. Coastal upwelling zones may be particularly sensitive, given that they have naturally low pH and may therefore be closer to biological thresholds under continued acidification.
3. Currently, in about 10% of the ocean volume, levels of dissolved oxygen drop below 88 μmol/kg [*Bianchi et al*., 2012], a condition defined as hypoxia. Many higher organisms such as crustaceans and fish cannot tolerate hypoxia for more than a brief period of time. As the climate warms, oxygen becomes less soluble in seawater, and so one might expect the volume of hypoxic waters to increase, potentially altering important marine ecosystems [*Matear and Hirst*, 2003]. Models generally predict significant deoxygenation under warming [*Schmittner et al*., 2008; *Frölicher et al*., 2009], but the patterns of oxygen loss vary significantly between models [*Bopp et al*., 2013].
4. Global warming is expected to increase the near-surface stratification. The death of biota in the well-lit ocean surface layer produces sinking organic detritus, removing the nutrients necessary to drive biological productivity. As a result, greater stratification increases the difficulty in resupplying nutrients to the surface in low latitudes, but also increasing the average level of light within the mixed layer. This is expected to cause an increase of productivity in high latitudes, but a decrease at low latitudes [*Bopp et al*., 2001; *Steinacher et al*., 2010], which may have significant impacts on the global distribution of fish harvest [*Cheung et al*., 2010].

Early 3-dimensional ocean biogeochemical models included a small number of explicit tracers, first representing only a single macronutrient element in its inorganic state with simple uptake kinetics [*Bacastow and Maier-Reimer*, 1990] and then supplementing this with a few interdependent tracers representing some combination of phytoplankton, zooplankton, bacteria, and detritus [e.g., *Sarmiento et al*., 1993; *Oschlies and Garçon*, 1999]. Each tracer in these models was "prognostic," including transport by the advection and mixing calculated by the ocean physics model, as well as a source/sink term reflecting nutrient uptake by phytoplankton, grazing by zooplankton, and production of detritus by sloppy feeding, feces, and mortality. The inclusion of each additional tracer typically increased the computational burden by on the order of 15% when using a level-coordinate ocean model with a flux-limited advection scheme, which was of minor importance for a small number of tracers.

In recent years, these simple biogeochemical models have given way to ecosystem models that follow the same principles but include far larger numbers of tracers. The increase in tracer number is driven by the desire to capture more biogeochemically important processes by explicitly representing multiple functional types of living organisms (e.g., N_2 fixers, diatoms, prochlorococcus, coccolithophorids, dinoflagellates etc., as well as multiple zooplankton size groups) and multiple nutrients (NO_3, NH_4, PO_4, Fe, and Si). If the stoichiometry of nutrient elements varies between organisms, it becomes necessary to include an additional tracer for each nutrient element, e.g., diatom-N, diatom-P, diatom-Fe, and diatom-Si.

The inclusion of such complex ocean biogeochemical modules within Earth System Models, however, comes into conflict with the demand for higher model spatial resolution. On land, such high resolution is required in order for the models to properly represent geographical features such as mountain ranges which modulate precipitation distributions and thus terrestrial ecosystems and carbon storage. In the ocean, resolution finer than 10 km is required to simulate the narrow continental shelves where many productive fisheries are located and where the impacts of acidification may be most intense [*Gruber et al*., 2012], as well as to capture some of the impacts of mesoscale oceanic eddies. Even finer ocean resolution is required to capture small-scale dynamical structures that have been shown to have an important role in modulating the seasonal cycle [*Mahadevan et al*., 2012]. However, "comprehensive" ocean biogeochemical modules such as those used by the major modeling centers increase the amount of resources required by the ocean component by an amount that can make high-resolution simulations unaffordable. For example, the Tracers of Ocean Productivity with Allometric Zooplankton (TOPAZ) code of *Dunne et al*. [2013], carries 30 prognostic tracers, which increases the total computational burden of the model fourfold.

In considering the value of large tracer numbers, it is useful to consider four things. First, even the most complex of ecosystem models is far simpler than the real marine ecosystem, which includes thousands of species, and whose internal dynamics exhibit chaotic behavior even in relatively simple experiments

[*Beninca et al*., 2008]. Second, there are few sufficiently detailed global data sets available with which to ground-truth the behavior of organic tracers carried in these ecosystem models: reliable, widespread observations are limited to inorganic dissolved chemicals, and satellite observations of chlorophyll and growth rates, leading to underdetermination of model parameters [*Ward et al*., 2010]. Third, the quantity of nutrient elements transported by the living organic phases is relatively small, given the small concentrations of organic pools, and can even be subject to inconsistency between multiple elements due to numerical approximations [*Christian*, 2007]. Fourth, it can be difficult to add new features such as stable isotopes and nutrient-tracking tracers, or to compute transport diagnostics, with a model that already includes many tracers of organic matter. Given these four factors, a large number of tracers are not necessarily beneficial, particularly when an estimate of the interactions between the ecosystem and the physicochemical environment is the fundamental aim, rather than the internal ecosystem dynamics themselves.

The need to balance the computational cost with ecosystem resolution has prompted prior works to compare biogeochemical models of varying tracer number in both 1-dimensional [*Friedrichs et al*., 2007] and 3-dimensional frameworks [*Kriest et al*., 2010; *Kwiatkowski et al*., 2014]. These prior studies spanned a heterogeneous array of models, with a range of ecological and biogeochemical approaches. They generally concluded that while the more complex models do not necessarily produce better simulations of annual-mean dissolved nutrients and gases, they do resolve more processes of interest [*Kwiatkowski et al*., 2014]. In addition, there is the possibility that a less-complex model may simply be better "tuned" to its physical model, and therefore produce a good simulation for the wrong reasons [*Friedrichs et al*., 2007].

This paper follows on from these prior studies to make the point that many of the most important and robust functional traits of complex models may be achieved with a relatively small number of tracers, and therefore small computational burden, by treating living biomass implicitly and parameterizing the net results of important "sub-ecosystem-scale" processes. The approach taken here is quite different than the prior works, in that we examine two simple models reverse-engineered from a complex model, rather than a suite of independent models. TOPAZ, one of the more complex models of the Coupled Model Intercomparison Project Phase 5 (CMIP5), is compared with two reduced-tracer models that nonetheless share some of the more complex aspects of the TOPAZ ecological formulation. These aspects include, among others, a representation of iron limitation, and the impact of grazing and water temperature on community size structure and export production. Thus, although we reduce the number of tracers back to those more typical of the early generation of three-dimensional ocean biogeochemical models [*Maier-Reimer*, 1993; *Sarmiento et al*., 1993], we attempt to maintain the more robust aspects of ecosystem functionality as resolved by contemporary, complex models.

2. Model Description

2.1. Full Ecosystem Model: TOPAZ

The TOPAZ code is that used in the GFDL ESM2M contribution to the IPCC Fifth Assessment Report. This model keeps track of five inorganic nutrients used by phytoplankton: nitrate, ammonia, inorganic phosphate, silicate, and dissolved iron. Additionally, the model carries three other dissolved inorganic tracers: dissolved inorganic carbon, alkalinity, and dissolved oxygen. Based on the work of *Dunne et al*. [2007], the model also keeps track of fine lithogenic material, which plays a role in ballasting organic material and delivering it to the sediment [*Armstrong et al*., 2001; *Klaas and Archer*, 2002]. The five inorganic nutrients are taken up in different ways by three classes of phytoplankton: small, large, and diazotrophic. A comprehensive description of TOPAZ v2 can be found in the supporting information of *Dunne et al*. [2013].

2.2. Parameterized Ecosystem Model: BLING

The Biogeochemistry with Light Iron Nutrient and Gas model version 0 (BLINGv0, hereafter simply BLING) was developed as a reduced-tracer biogeochemical tool which would nonetheless retain many of the functional relationships developed for TOPAZ. A full description is available in *Galbraith et al*. [2010]. In brief, the main simplifications include:

1. Reducing the number of nutrients. Given the very small concentration of ammonium in the environment, and the strong correlation between nitrate and phosphate in seawater (outside of denitrifying oxygen minimum zones), the limitation of growth by macronutrients is simplified to a single macronutrient

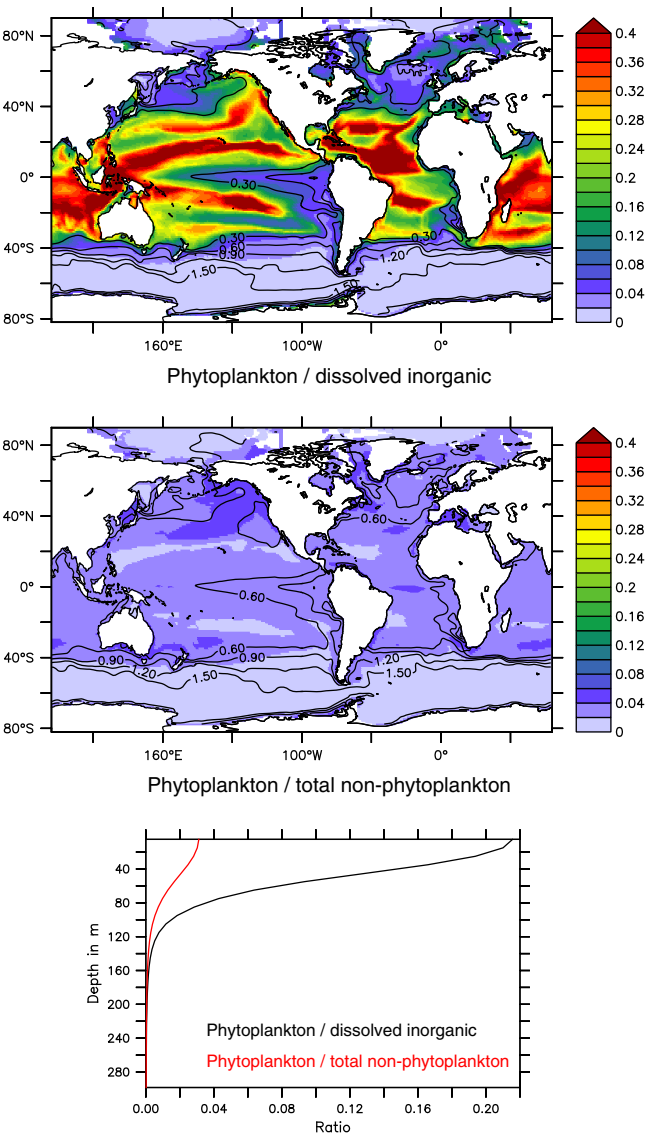

Figure 1. Macronutrient partitioning between phytoplankton biomass, dissolved inorganic, and total nonphytoplankton pools. All values are averaged over years 1921–1922 of the TOPAZ simulation. (top and bottom) Phytoplankton biomass is equal to the Redfield-weighted average of N and P in all three phytoplankton groups, and compared to the similarly weighted PO_4 and NO_3 ("inorganic") and (middle and bottom) the weighted PO_4 and NO_3 plus heterotrophic bacteria, labile DON, and semilabile DON and DOP ("non-phytoplankton"). (top, middle) Averages are calculated over the upper 50 m of the water column. Contours show the "average macronutrient" concentration, $PO_4/2 + NO_3/32$.

tracer. This tracer is called "PO_4," since there is no N_2 fixation or denitrification, although its role as the primary limiting macronutrient makes it more like NO_3. Dissolved iron is also included as a prognostic tracer, given its role as a limiting nutrient throughout the biogeochemically important High Nitrate Low Chlorophyll (HNLC) regions [*Moore et al.*, 2013]. As a scavenged trace metal with a short residence time, its dynamics are very different than those of "PO_4," therefore requiring explicit simulation.

2. Replacing the dependencies of nutrient limitation on cellular elemental quotas by assuming that nutrient limitation is defined by the in situ dissolved concentrations in the ambient seawater. Thus, overall nutrient limitation is represented simply as the minimum of two saturating hyperbolic (Michaelis-Menten) functions, one for each of PO_4 and Fe. In addition, the effect of Fe limitation on the phytoplankton photosystem is simulated through a change in light-harvesting efficiency and chlorophyll synthesis.
3. Inferring the biomass of small and large phytoplankton as a function of growth rate, following the empirically calibrated grazing law of *Dunne et al.* [2005]. This parameterization reflects the idea that the biomass of large phytoplankton is more sensitive to changes in growth rate than is the biomass of small phytoplankton. Importantly, the parameterization assumes the ecosystem growth and mortality rates are balanced, which may be true under most conditions, but breaks down during seasonal blooms. The biomass term is carried as a diagnostic tracer (i.e., a 3-dimensional array that is not subject to ocean advection and mixing, and therefore has a tiny computational cost), smoothed over a multiday timescale, to prevent very fast adjustments of the biomass to sudden change in growth conditions (most importantly the diurnal cycle). Instantaneous uptake is then calculated from the instantaneous growth rates multiplied by the diagnostic biomass concentration.
4. Allowing for only one pool of organic phosphorus that is subject to advection, which we call "dissolved organic material" (DOP) for ease of notation, whose source is determined as a nonlinear, empirically calibrated function of the instantaneous growth rate. The inclusion of an advected organic pool alleviates, to some degree, the lack of living organic matter transport by providing a means by which noninorganic nutrient can be transported by ocean circulation.

5. Using a simple model for sinking organic matter, which ignores the lithogenic pools and mineral ballasting. Remineralization of sinking particles is calculated implicitly, instantaneously distributing the remineralization products throughout the full water column assuming a constant remineralization rate and a sinking rate that increases with depth.

As a result of these changes, the total number of prognostic tracers in BLING is reduced from 30 to 4 core tracers (phosphate, iron, dissolved organic phosphorus, and oxygen) with the option to include two carbon cycle tracers (Dissolved Inorganic Carbon, DIC, and alkalinity) [*Bernardello et al*., 2013].

The removal of prognostic phytoplankton tracers introduces an error, in that the transport of elements as components of living organic matter is no longer resolved. The degree to which this will affect macronutrient transport within the ocean can be estimated using the comprehensive model TOPAZ, by examining the relative concentrations of macronutrients in living biomass (i.e., the sum of all N and P contained in phytoplankton) with the total dissolved inorganic macronutrients (NO_3 and PO_4), and the sum of all nonphytoplankton pools (i.e., NO_3 and PO_4 plus dissolved organic nutrients, semilabile DON and DOP, heterotrophic bacteria and labile DON). These are shown as ratios in Figure 1. As predicted by TOPAZ, the stock of nutrient elements in living phytoplankton is less than 10% of the inorganic nutrient concentration in surface regions where inorganic nutrients are present in significant concentrations (top). In oligotrophic waters that are starved for macronutrient, this ratio can become significantly higher, exceeding 40% of the inorganic nutrient concentration in the subtropical gyres. However, when we consider the stock of total nonphytoplankton nutrient pools (middle), which includes dissolved organic matter and heterotrophic bacteria, the relative contribution of living phytoplankton is very small throughout the oceans, generally less than 5%. Furthermore, as shown in the bottom plot, the proportion of macronutrients stored in living tissue decreases rapidly with depth, becoming negligible below the surface mixed layer. Thus, the transport of macronutrient in the surface mixed layer of the global ocean is represented reasonably well in BLING by including the DOP tracer.

Although most of the important governing equations are similar between TOPAZ and BLING, a number of the biological parameters do differ. In particular, no distinction is made in the uptake affinities or growth parameters between large and small phytoplankton; this is not necessarily the case, but was an arbitrary choice to reduce the number of model parameters. In addition, there was no attempt to tune the parameters controlling sinking particle remineralization in BLING in order to match the TOPAZ profiles, leading to a fundamental difference in the regeneration of nutrients with depth. It should also be mentioned that the production of $CaCO_3$ in BLING is only calcite and occurs in fixed proportion to the inferred small phytoplankton primary production, and the alkalinity inventory is held constant, in contrast to the more complex alkalinity cycle in the default version of TOPAZ.

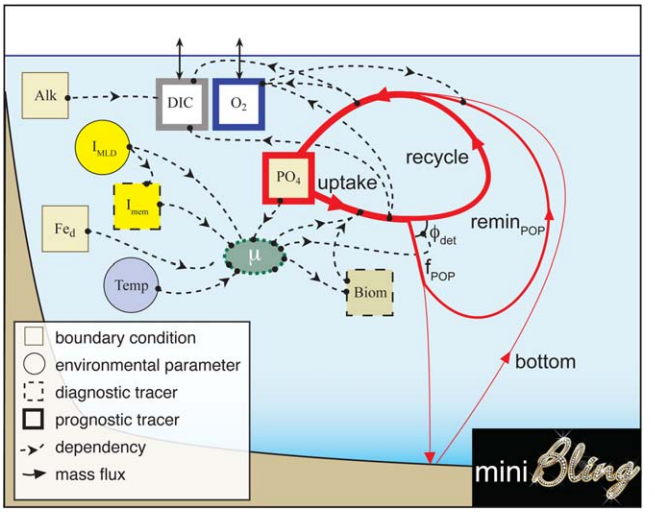

Figure 2. Schematic of miniBLING. *Alk* is alkalinity, I_{MLD} is the local irradiance (averaged vertically within the mixed layer), I_{mem} is equal to I_{MLD} with a multiday smoothing to represent photoadaptation, Fe_d is a climatological dissolved iron concentration, *Temp* is the local water temperature, μ is the growth rate, *Biom* is the biomass of phytoplankton, ϕ_{det} is the fraction of organic matter produced that goes to sinking detritus, f_{POP} is the sinking flux of detrital P, *recycle* is the fast recycling of organic matter to PO_4, $remin_{POP}$ is the remineralization of sinking particles to PO_4, *bottom* is the remineralization of sinking particles to PO_4 at the seafloor.

2.3. Minimal Tracer Model: miniBLING

The miniBLING model, described here for the first time and shown schematically in Figure 2, represents the minimum possible number of prognostic tracers: only one prognostic biological tracer is required, named PO_4 (representing a general macronutrient, as in BLING). This extreme tracer minimization is achieved relative to BLING by:

1. Removing the dissolved organic matter tracer (DOP). With no dissolved organic matter to remineralize, the drawdown of PO_4 to tiny values in oligotrophic regions

could cause numerical problems. To represent the uptake of nonexistent PO_4 under oligotrophic conditions, an additional term, PO_{4min}, was added to prevent uptake of a small, inaccessible fraction of PO_4, equal to 0.01 μM. In addition, the recycling of P under very low PO_4 concentrations within surface waters was accelerated by multiplying the fraction of particulate organic matter produced from photosynthesis by $PO_4/(k_{PO4recycle}+PO_4)$ where $k_{PO4recycle}$ was set to a value of 0.02 μM.

2. Removing the prognostic iron tracer. Instead, a climatological map of monthly varying iron concentrations over the upper 100 m was used, generated from a well-equilibrated simulation with BLING. This provides large-scale iron gradients between iron-rich regions such as the subtropical North Atlantic, and iron-depleted regions such as the Southern Ocean. However, it decouples the iron concentrations from their utilization, which can lead to unrealistic behavior, particularly given changes in ocean circulation (see section 3.2).
3. Removing the alkalinity tracer. Instead, the sea surface alkalinity is calculated as a function of sea surface salinity, using an empirical linear regression of observed sea surface alkalinity [*Key et al*., 2004] versus salinity. The regression uses local ratios of alkalinity/salinity relative to an intercept of 400 μM, allowing the alkalinity at each grid cell to vary according to the hydrological cycle, but ignoring any possible change in the distribution of calcification or remineralization. The cycling of $CaCO_3$ is therefore removed as well.

The empirical parameterizations of biomass and organic matter cycling used in BLING, as described above and in *Galbraith et al*. [2010] are retained, implicitly simulating a community with two sizes of phytoplankton and grazers, and with a temperature and growth-rate-dependent export fraction.

Beyond the one required prognostic tracer, two optional tracers are also included in the simulations shown here: dissolved oxygen and dissolved inorganic carbon. The code for these tracers is identical to that used for BLING.

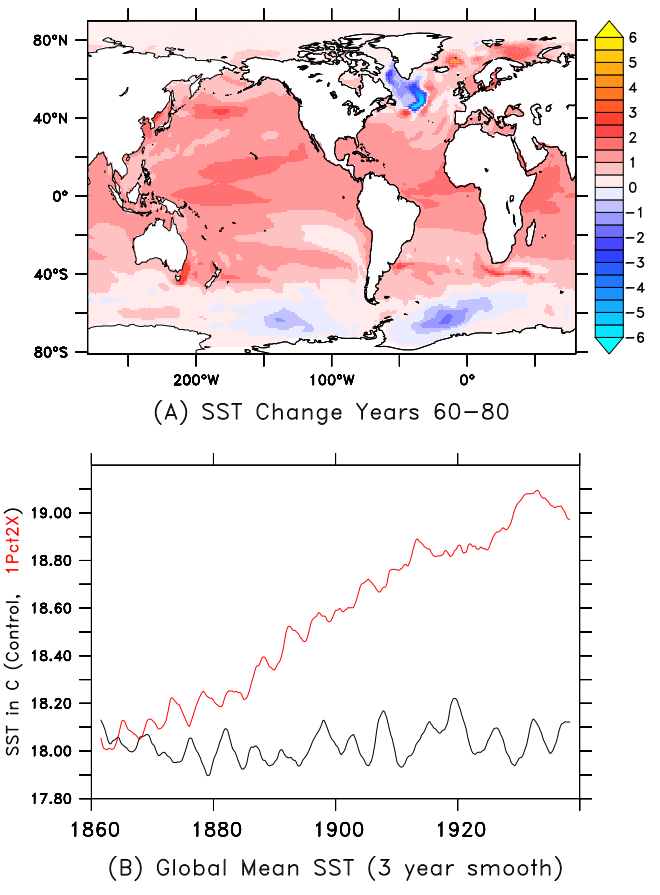

Figure 3. Ocean warming in the idealized CO_2 increase. (a) The spatial pattern of warming during years 60–80 of the CO_2 doubling simulation, relative to the corresponding years of the control simulation, in degrees C. (b) The global mean sea surface temperature over the 80 year control (black) and CO_2 doubling (red) simulations.

2.4. Physical Model and Scenarios

The three ocean biogeochemical modules are embedded in the ESM2M Earth System Model, and integrated simultaneously. Thus, they experience exactly the same physical environment. The model has an atmosphere with nominal 2° resolution and an ocean with nominal 1° resolution, with meridional resolution increasing to as fine as 1/3° near the equator. The chlorophyll used to calculate shortwave absorption in the ocean model is taken from the simulation with TOPAZ, so that there is no self-shading feedback in the BLING or miniBLING runs. Full documentation on the basic model simulations is provided in *Dunne et al*. [2012].

The model was initialized with temperature and salinity from the end of a prior 2400 year simulation, and with biogeochemical tracers from World Ocean Atlas and GLODAP. The model was run for 100 years with the solar constant, greenhouse gasses, and aerosols all fixed at preindustrial, year 1860 values. At this point, the simulation was branched into two 80 year simulations. The first maintained constant year 1860 boundary conditions, referred to as the preindustrial control.

The second simulation was identical, except that the atmospheric CO_2 increased at a rate of one percent/year over a 70 year period, after which the CO_2 is twice its initial value, and then held constant for 10 years. At the end of the idealized CO_2 doubling simulation, the increase in global SST is 1°C (Figure 3).

3. Results

3.1. Preindustrial Simulation Chemistry

We begin by examining the simulations of the three models under identical preindustrial conditions, by comparing them with chemical parameters for which extensive observations exist: macronutrient, oxygen, and dissolved inorganic carbon. Because the total simulation length was only 180 years, it is not fully equilibrated. However, our focus is on the comparison between models, rather than the equilibrated states of the models themselves, for which the relative trajectories from the common initialization state indicate model differences. In addition, we focus on the surface ocean and upper part of the water column, which equilibrates more rapidly. We first consider macronutrients.

Given that BLING includes only one macronutrient to capture the overall effects of both nitrate and phosphate, we follow *Galbraith et al.* [2010] in comparing the models to an average macronutrient, with the nitrate concentration scaled by the approximate Redfield ratio of 16: $(PO_4 + NO_3/16)/2$. With TOPAZ, the simulated average of PO_4 and NO_3 is directly compared to the observed average macronutrient, whereas in BLING and miniBLING we compare to the modeled "PO_4" macronutrient. As shown in Figure 4a, all three models have strong correlations with the observed global pattern of surface macronutrients, with high values in the Southern Ocean, intermediate values in the northern subpolar regions and at equatorial upwellings, and low values in the gyres. The global pattern of error (Figures 4b and 4c) generally shows nutrient

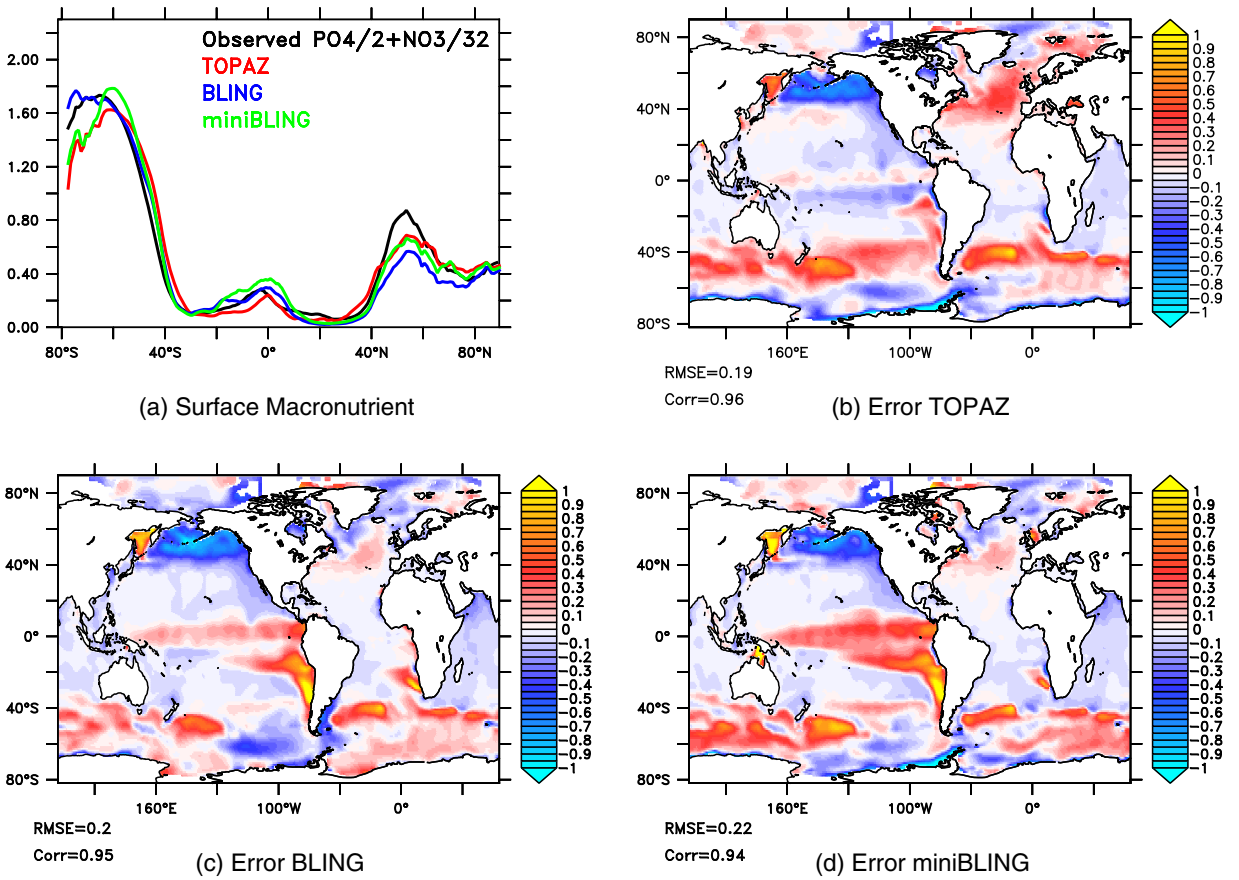

Figure 4. Surface macronutrient concentrations. Observations [*Garcia et al.*, 2014a] are compared with the three models in the top (0-10 m) ocean level. (a) Zonal average of the observed average macronutrient, $PO_4/2+NO_3/32$, and the simulated average macronutrient (TOPAZ) or the simulated PO_4 (BLING, miniBLING). (b,c,d) Difference between the observed macronutrient concentration and the simulated concentrations, within the upper 10 m. All units are μM.

concentrations that are too low in the North Pacific, particularly the subarctic gyre and Bering Sea (but too high in the Sea of Ohkotsk) and too high in the mode water formation regions in the Southern Ocean. Although there are significant differences in surface macronutrients between the three models, these differences do not show a consistent trend as one moves to fewer tracers. Both TOPAZ and miniBLING, for example, show the highest values of phosphate concentrated away from the Antarctic margin, while BLING remains high all the way to the continent (Figure 4a). The three models have essentially indistinguishable errors, as quantified by RMSE and correlation coefficient (Figure 4).

The oxygen fields simulated by the three models are also quite similar. As shown in Figure 5, at depths between 200 and 600 m, the models all tend to overpredict the amount of tropical hypoxia, failing to capture the local high in oxygen along the equator and underestimating oxygen in both the tropical Atlantic

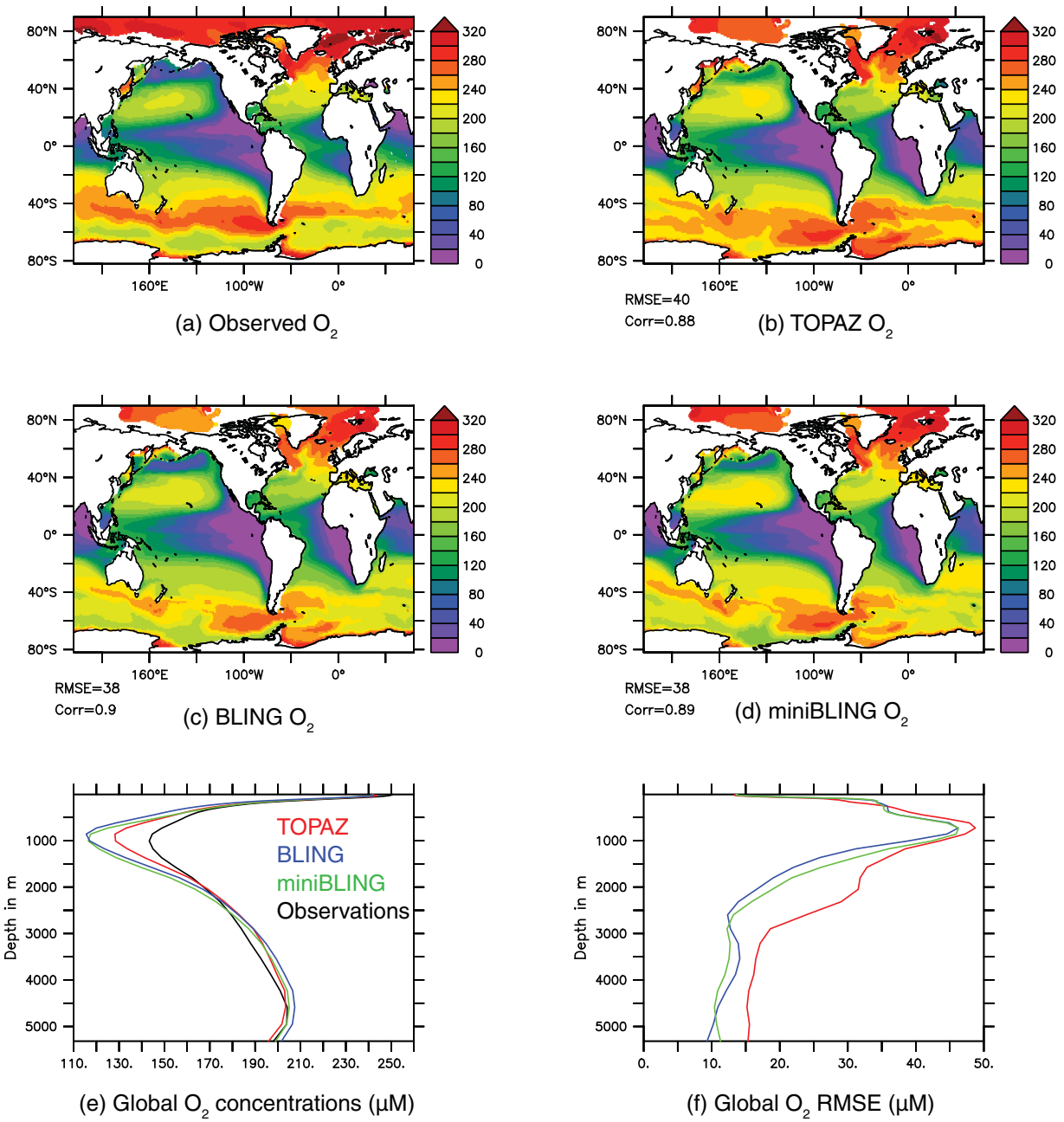

Figure 5. Subsurface oxygen concentrations. Observations [*Garcia et al.*, 2014b] are compared with the three models over the depth range 200-600 m, where the strongest oxygen minimum zones are found. Correlation coefficients and root mean squared error are calculated from the 3-dimensional oxygen fields over this depth range. All units are μM.

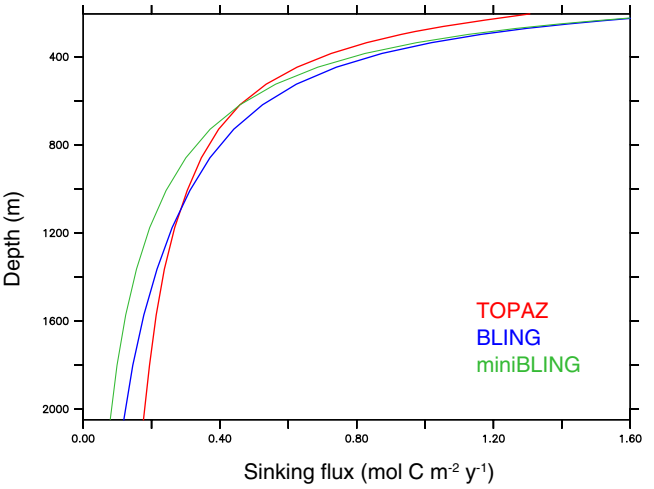

Figure 6. Organic matter remineralization. The global, horizontally averaged sinking flux of particulate organic carbon is shown for each of the three models.

and Bay of Bengal. The general underprediction of oxygen at tropical mid depths is likely, at least in part, a result of lateral mixing that is too weak: as discussed in *Gnanadesikan et al.* [2013], the lateral diffusive supply of oxygen is underestimated by coarse resolution models that cannot resolve the tropical zonal jets [*Dietze and Loeptien*, 2013; *Duteil et al.*, 2014]. In contrast, TOPAZ tends to overestimate oxygen concentrations in the North Pacific, where ESM2M is known to ventilate too strongly [*Dunne et al.*, 2013], whereas BLING does a significantly better job in this region and tends to underestimate oxygen concentrations slightly in the Antarctic mode and intermediate waters. The net result is that simulated oxygen in BLING correlates with the observations slightly better than in TOPAZ, but again the errors are so similar between the three models as to be essentially indistinguishable. The correlation coefficients place all three models squarely at the center of the pack for performance among the CMIP5 models, as summarized in Figure 2 of *Bopp et al.* [2013].

Looking at the vertical profiles of mean oxygen (Figure 5e) and RMS oxygen error (Figure 5f), we see that BLING and miniBLING tend to produce a more intense minimum than observed around 1000 m, but have lower RMS error over all, so that the pattern of oxygen is more realistic at all depths below 400 m. This contrast can be attributed to the difference in remineralization profiles, evident from the sinking carbon fluxes shown in Figure 6. The BLING and miniBLING model fluxes are higher at shallow depths, but decrease more rapidly with depth, reflecting faster remineralization rates relative to sinking rates, with the fastest rates in BLING, causing rapid oxygen consumption in the upper ocean. Both remineralization rates and sinking rates vary widely within the global ocean, for reasons that remain incompletely understood [*Marsay et al.*, 2015], so that it is very difficult to know what the most appropriate values of these important parameters should be. The fact that the remineralization rates differ between BLING models was due to choices during model development and the lack of any representation of mineral ballasting, rather than reflecting a fundamental feature of tracer number.

Finally, we briefly examine the carbon cycle in the three models, compared to the preindustrial estimate of GLODAP [*Key et al.*, 2004]. Figure 7 shows the global distributions of DIC from 200 to 600 m, the same depth range as for oxygen in Figure 5. Because the equilibration timescale for DIC is an order of magnitude slower than it is for oxygen, it would be expected that the DIC concentrations would require multiple centuries to near a steady state, much longer than the simulation analyzed here. Nonetheless, the relative differences between models provide an indication of how the three would likely differ at equilibrium. All models show excessive DIC in the eastern tropical Atlantic, consistent with a buildup of respired carbon due to the lack of ventilation by zonal jets. In addition, all models fail to reproduce the observed north-south asymmetry in the westward extent of high-DIC waters in the tropical Pacific, a bias likely linked to bias in the physical model's representation of the Intertropical Convergence Zone (ITCZ). The BLING models have higher DIC concentrations than TOPAZ in the subarctic Pacific and Antarctic, consistent with greater storage of respired organic carbon as also indicated by the lower oxygen concentrations. Despite their differences, as noted above for oxygen and macronutrients, the correlation coefficients between simulated DIC and GLODAP are essentially identical between the three models.

We note that, using TOPAZ with ocean models of the same horizontal resolution but different vertical coordinates, *Dunne et al.* [2013] and *Gnanadesikan et al.* [2014] found differences in the biogeochemical state that were at least as large as the differences between TOPAZ and the BLING models considered here. Similar results, showing that a given biogeochemical model can produce quite different annual mean

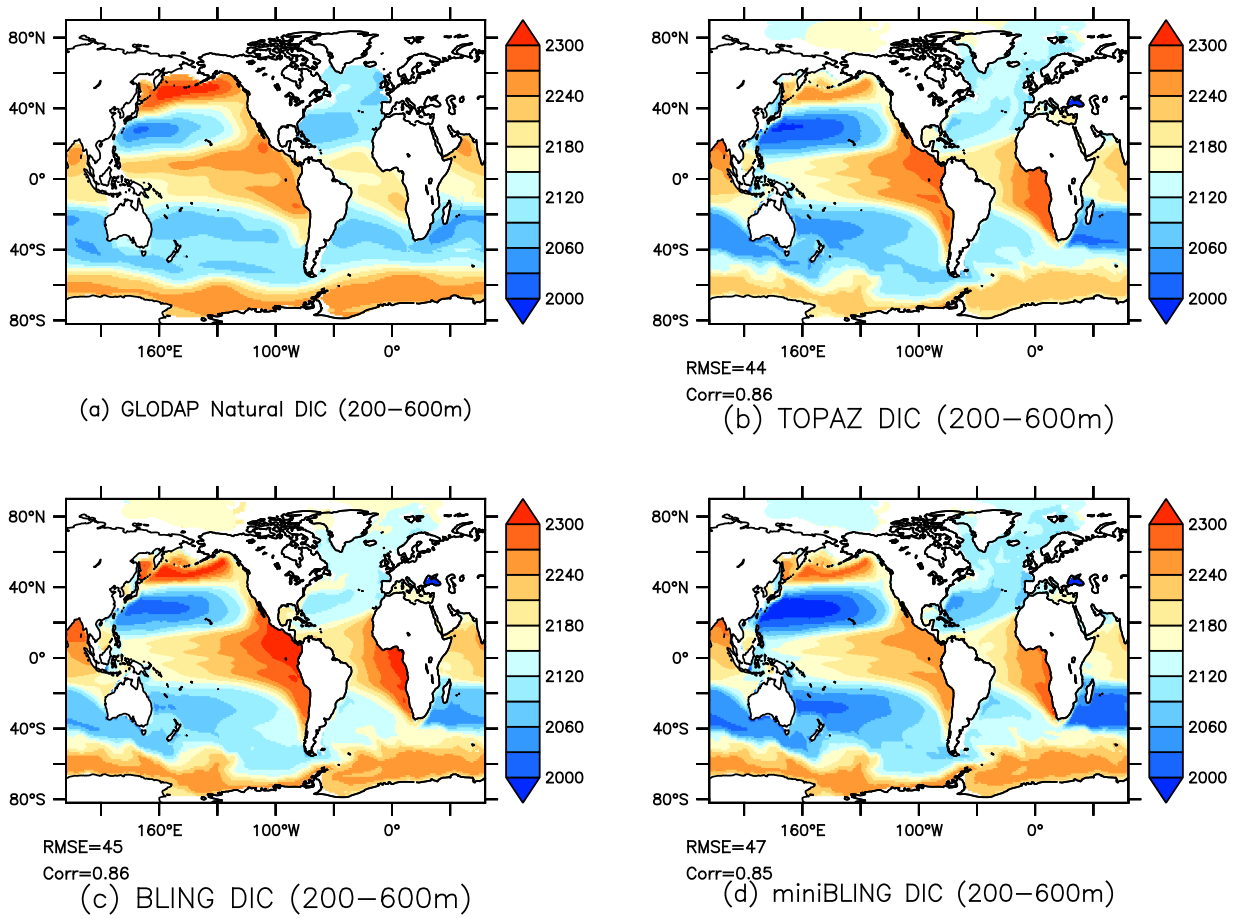

Figure 7. Subsurface DIC concentrations. An observational estimate of preindustrial DIC [*Key et al*., 2004] is compared with the three models over the 200–600 m depth range. Correlation coefficients and root mean squared error are calculated from the 3-dimensional fields over this depth range. All units are μmol kg^{-1}.

simulations depending on the choice of physical ocean model, have been reported by *Sinha et al*. [2010] and *Séférian et al*. [2013]. These findings, when contrasted with the minimal differences apparent between TOPAZ and the BLING models, would appear to highlight the importance of using a realistic ocean circulation model over an ecosystem model with a large number of tracers.

3.2. Looking Under the Hood: Biological Cycling

From the above analysis, TOPAZ, BLING, and miniBLING appear to yield extremely similar results, suggesting that large-scale biogeochemical cycling can be estimated very well at the global scale with a small number of tracers, provided appropriate parameterizations for the functional impact of unresolved components such as living biomass and dissolved iron concentrations. We now turn to the question of whether this is simply because the biological cycling in the models is very similar.

Figure 8 shows the global pattern of sinking organic matter for the models, averaged annually at 105 m depth, compared with an observation-based estimate of export derived from satellite ocean color and temperature [*Dunne et al*., 2007]. Compared with the macronutrient and oxygen concentrations, the spatial pattern of export agrees less well with the observational estimate, with significantly lower correlation coefficients. This may be due, in part, to larger uncertainties in the observational estimate of export. However, there are also much larger intermodel differences than found with the chemical concentrations. The TOPAZ model is closest to the observations, with the main differences being a modest overestimate of open-ocean export at low latitudes, and an underestimate of export in the northern high latitudes. The BLING models show a greater range between regions of high and low export, with export that is actually too high in the northern high latitudes and much too high in the Southern Ocean. All three models display

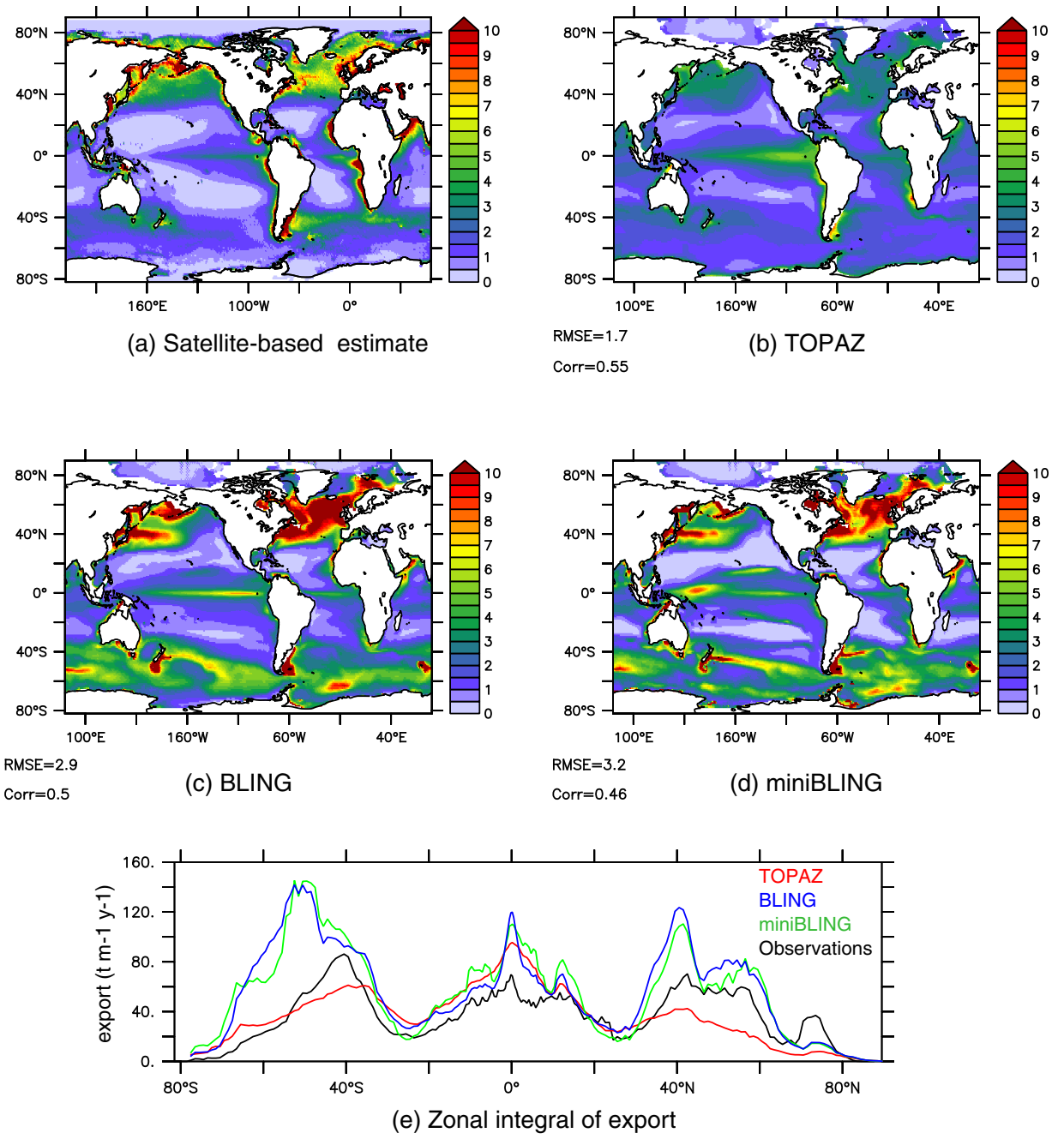

Figure 8. Organic matter export fluxes. "Observations" are the satellite-derived organic export flux from *Dunne et al.* [2007]. Model export fluxes are calculated at 105 m depth. All units are mol C m^{-2} yr^{-1}.

an overly broad latitudinal spread of export in the central tropical Pacific, but this is particularly pronounced in miniBLING, which actually shows elevated bands of export flanking the equator at 10–20° latitude; we return to these tropical export bands below.

Looking first at the high latitudes, we focus on the North Atlantic, where the BLING models show much more export than TOPAZ. Figure 9a shows the seasonal cycle of surface macronutrient concentrations for the three models, compared to observations. The general shapes of the macronutrient curves are remarkably similar to each other, and to the observations, with similar amplitudes. The BLING model tends to underestimate summer concentrations, but does well during the winter, while TOPAZ overestimates the winter concentrations, but does well with the summer. However, we see that these modest differences in

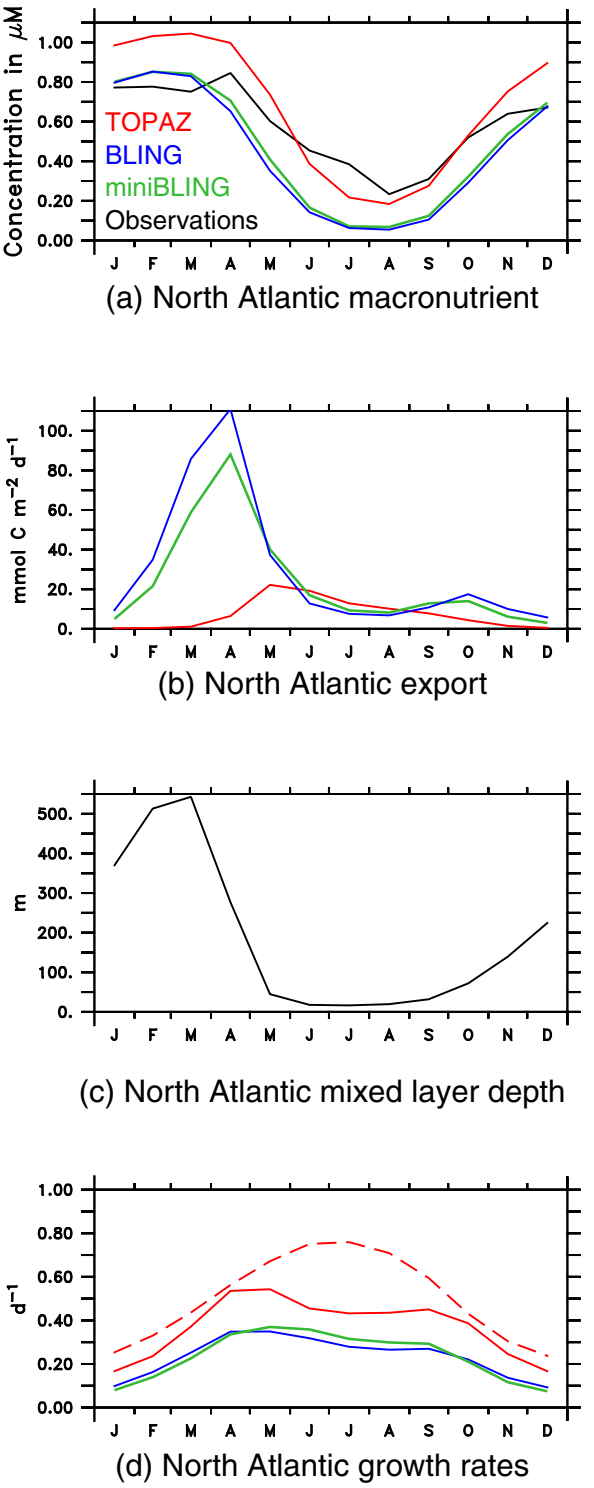

Figure 9. Seasonal cycle in the North Atlantic surface ocean. Values in (a) and (d) are shown for the top layer, the export in (b) is calculated at 105 m depth, and all plots show averages over the region 50–60 N, 30–50 W. Note that the macronutrient is equal to $PO_4/2+NO_3/32$. In Figure 9d, the solid red line shows the TOPAZ large phytoplankton growth rate, while the dashed red line shows the TOPAZ small phytoplankton growth rate.

macronutrient concentrations actually belie a dramatic difference in the models, which is evident from the export fluxes. The BLING models simulate extremely strong blooms (roughly fivefold the TOPAZ bloom) that start very early, in February rather than April (Figure 9b). How can such differences in bloom export occur, given the identical ocean physics and similar macronutrient concentrations? The answer lies in Figure 9c, which shows the mixed layer depth. Because the mixed layer is still hundreds of meters deep when the BLING blooms occur, there is huge available source of nutrients—essentially, the bloom is tapping into a massive reservoir of nutrients, which supports a huge export flux. The TOPAZ bloom, in contrast, occurs when the North Atlantic is already stratified, and is therefore limited by the nutrient reservoir available in the relatively small mixed layer.

The different bloom timings can be attributed to the choice of a steady-state ecosystem balance in these versions of the BLING models. Because the biomass is determined by the environmentally dependent growth rate, it can adjust very quickly to an improvement in growth conditions. Unlike TOPAZ, in which the biomass of large phytoplankton must explicitly grow its way back from very low wintertime concentrations through photosynthesis in order to produce a bloom, the implicit BLING, and miniBLING biomass could potentially increase at rates that exceed the production of organic matter by photosynthesis. The blooms in BLING and miniBLING also receive an additional boost because the light absorption in the water column uses the chlorophyll predicted by TOPAZ, which does not increase until later in the spring. As a result, the average irradiance within the mixed layer during the early bloom is higher than it should be. The fact that the dramatic differences in bloom dynamics have little impact on global oxygen and nutrient cycling reflects the typically close balance between phytoplankton growth and loss in fully prognostic models like TOPAZ, as well as the importance of the surface properties during deep water formation, through their control of preformed nutrients [*Stommel*, 1979].

If only the phytoplankton growth dynamics differed between the models, rapid export

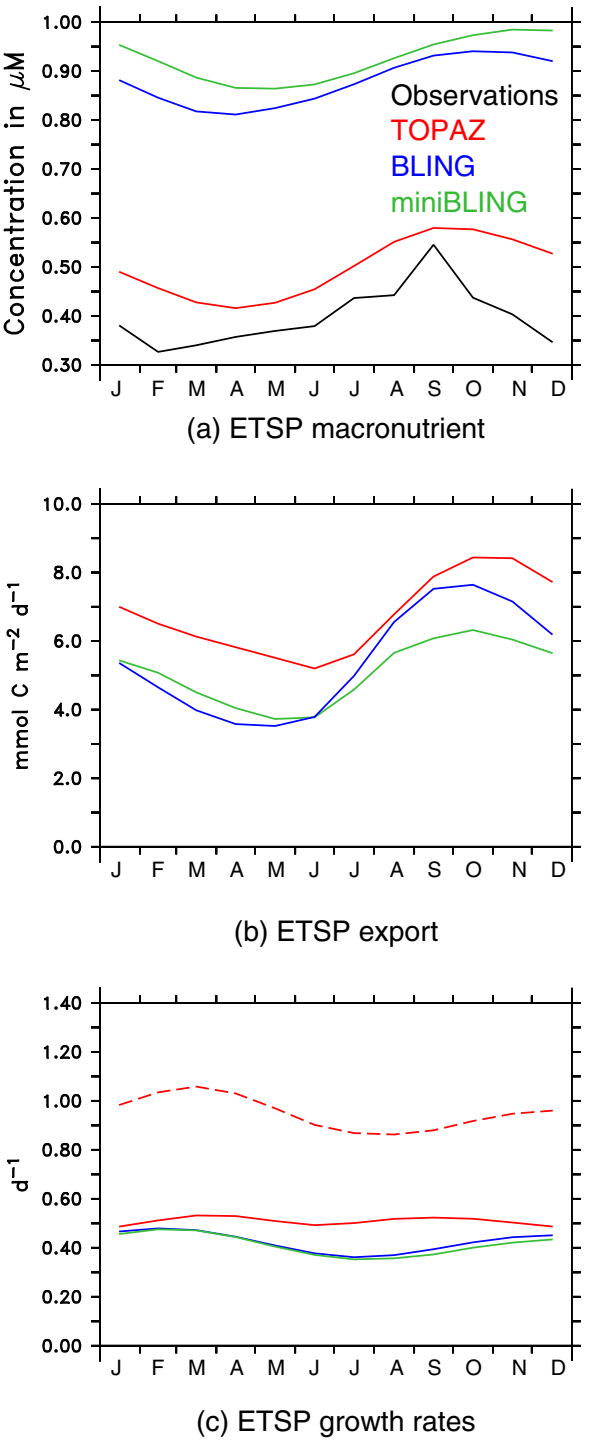

Figure 10. Seasonal cycle in the eastern Tropical South Pacific surface ocean. Values in (a) and (c) are shown for the top layer, the export in b is calculated at 105 m depth, and all plots show averages over the region 10–20 S, 60–110 W. In Figure 10c, the solid red line shows the TOPAZ large phytoplankton growth rate, while the dashed red line shows the TOPAZ small phytoplankton growth rate.

from the BLING models during the early bloom would be expected to deplete the North Atlantic surface waters of nutrients. However, the relatively shallow remineralization depth discussed above, which was chosen for the BLING models, helps to maintain a large subsurface nutrient pool in spite of rapid export: the wintertime macronutrient gradient between 10 and 400 m depth is 0.38 μmol m^{-4} in the BLING models, versus 0.20 μmol m^{-4} in TOPAZ. Thus, the early bloom is compensated by the shallow remineralization profile, which provides a large shallow nutrient pool to support the rapid export, while maintaining similar late-winter surface water properties. Because the models have similar surface water chemical properties during the critical period of deep water formation, the large-scale biogeochemical cycling is relatively insensitive to the bloom dynamics.

Turning to the low latitudes, we see a second important discrepancy between the models. As shown by Figure 10a, which takes the Eastern Tropical South Pacific (ETSP) as an example, the amplitude and timing of the seasonal cycles in macronutrient concentrations are quite similar between the models. However, while the concentrations in TOPAZ agree quite well with observations, the concentrations in the BLING models are significantly higher. This reflects slower export production in the BLING models, as shown by Figure 10b. This reduced export reflects slower growth rates, due largely to the fact that the BLING models used here do not resolve the different growth parameters of small versus large phytoplankton: the small phytoplankton of TOPAZ grow much faster in tropical waters, thereby supporting more rapid export (Figure 10c).

The miniBLING tropical export bands, clearly evident in Figure 8, turn out to be caused by the high tropical macronutrient concentrations, combined with the fact that iron is not carried as a prognostic variable. Rather, the iron concentrations are imposed as a climatological map, derived from the BLING model in a prior simulation. The BLING iron cycle causes surface iron concentrations to be very low where macronutrients are upwelled in the equatorial Pacific, since the strong export flux (supported by abundant upwelled macronutrient) scavenges iron out of the surface waters, leading to strong iron limitation. In contrast, in the subtropical gyres, macronutrient limitation prevents export, reducing scavenging,

and allowing higher iron concentrations to accumulate. This is particularly true in the northern subtropical gyre, where iron is delivered by Asian dust. The export bands occur on the transition between these domains, where macronutrient-rich waters in miniBLING are transported out of the iron-limited domain on a seasonal basis, and encounter externally applied higher iron concentrations. The combination of nonlimiting iron concentrations with abundant macronutrient fuels rapid growth pulses, which drive unrealistically large export within these bands.

Nevertheless, despite the tropical export bands, ocean interior dissolved oxygen is extremely similar between the models. This would appear to result from the fact that, in all cases, upwelled macronutrient is completely consumed within the tropics overall, closing the biogeochemical loop, and maintaining the same total oxygen consumption rates. The fact that the oxygen consumption is distributed over a different area in the BLING models appears to be largely compensated by the homogenizing effect of ocean circulation, leading to similar oxygen concentrations among the three models. We note that all models suffer equally from the lack of Tsuchiya jets, which are thought to play an important role in the real world by transporting relatively well-oxygenated waters eastward along the equator, and can only be resolved at ocean resolutions of 0.25° or better [*Dietze and Loeptien*, 2013].

It is important to emphasize that neither the high latitude nor the low latitude shortcomings of the BLING models is likely to be an inescapable consequence of reduced tracer number. The early bloom issue could perhaps be addressed by altering the light limitation parameters, or by including a diagnostic tracer for large phytoplankton biomass that would explicitly keep track of the change in biomass resulting from growth and mortality. The low latitude issue could be addressed by adding growth parameters to resolve a "small" phytoplankton type that grows quickly under such conditions, included within the subecosystem parameterizations. It seems likely that with some further effort, the performance of the BLING models could be brought even closer to that of TOPAZ.

3.3. Chemical Response to Anthropogenic Climate Warming

Given that the models have similar large-scale biogeochemical characteristics, despite differences in seasonal cycling, we now consider how these models respond to the idealized increase in anthropogenic carbon dioxide. The change in oxygen is shown in the left-hand column of Figure 11. All of the models simulate a loss of oxygen from the ocean of 2.1 μM in the global average, with large decreases at high latitudes, but increases in the equatorial region and in the deep ocean. The patterns of change are quite well correlated, with the global patterns between BLING and TOPAZ showing a correlation of 0.96 and the global pattern between miniBLING and TOPAZ a correlation of 0.93. All the models show a decline of oxygen in subpolar regions at around 500 m, driven in large part by declines in convection in the Weddell Sea, Ross Sea, Labrador Sea, Bering Sea, and Kuroshio Extension. The larger increases of oxygen in the tropical thermocline in BLING and miniBLING relative to TOPAZ are most pronounced in the western tropical Pacific, where BLING and miniBLING show increases up to 20 μM while TOPAZ is about half that. In the deep ocean, TOPAZ predicts a weak increase in oxygen concentrations (about 1 μM in the global ocean) while BLING and miniBLING predict weak decreases. This contrast is dominated by the difference in remineralization schemes between the models, rather than being a necessary consequence of the number of tracers.

The three models also show extremely similar patterns of uptake of anthropogenic carbon (right-hand column, Figure 11), with correlations between depth-integrated uptake in BLING and miniBLING and TOPAZ exceeding 0.99. The total amount taken up does, however, vary between the models, with TOPAZ producing the highest uptake of 326 Pg C, while BLING produces an uptake of 311 Pg C and miniBLING only 306 Pg C. Examining the zonal mean (not shown) we find that the models produce essentially identical results poleward of about 50° latitude in both hemispheres. The largest differences in inventory are found at the centers of the subtropical gyres. These in turn are associated with changes in alkalinity, which are larger in TOPAZ than in either BLING or miniBLING. The sea surface alkalinity determines how much of the total DIC is in the form of dissolved CO_2 gas, such that higher alkalinity causes a greater uptake of DIC. The production of calcium carbonate shells by calcifying plankton draws alkalinity out of the surface water, and sinking of the shells transfers the alkalinity to depth, reducing the surface ocean's ability to store carbon. In TOPAZ, the decrease in the saturation state of calcite and aragonite due to ocean acidification reduces the production of calcium carbonate in the surface layer, and causes sinking calcium carbonate to dissolve more rapidly. As a result, surface alkalinity is raised by 20 μM, while deep carbonate burial is decreased, causing the

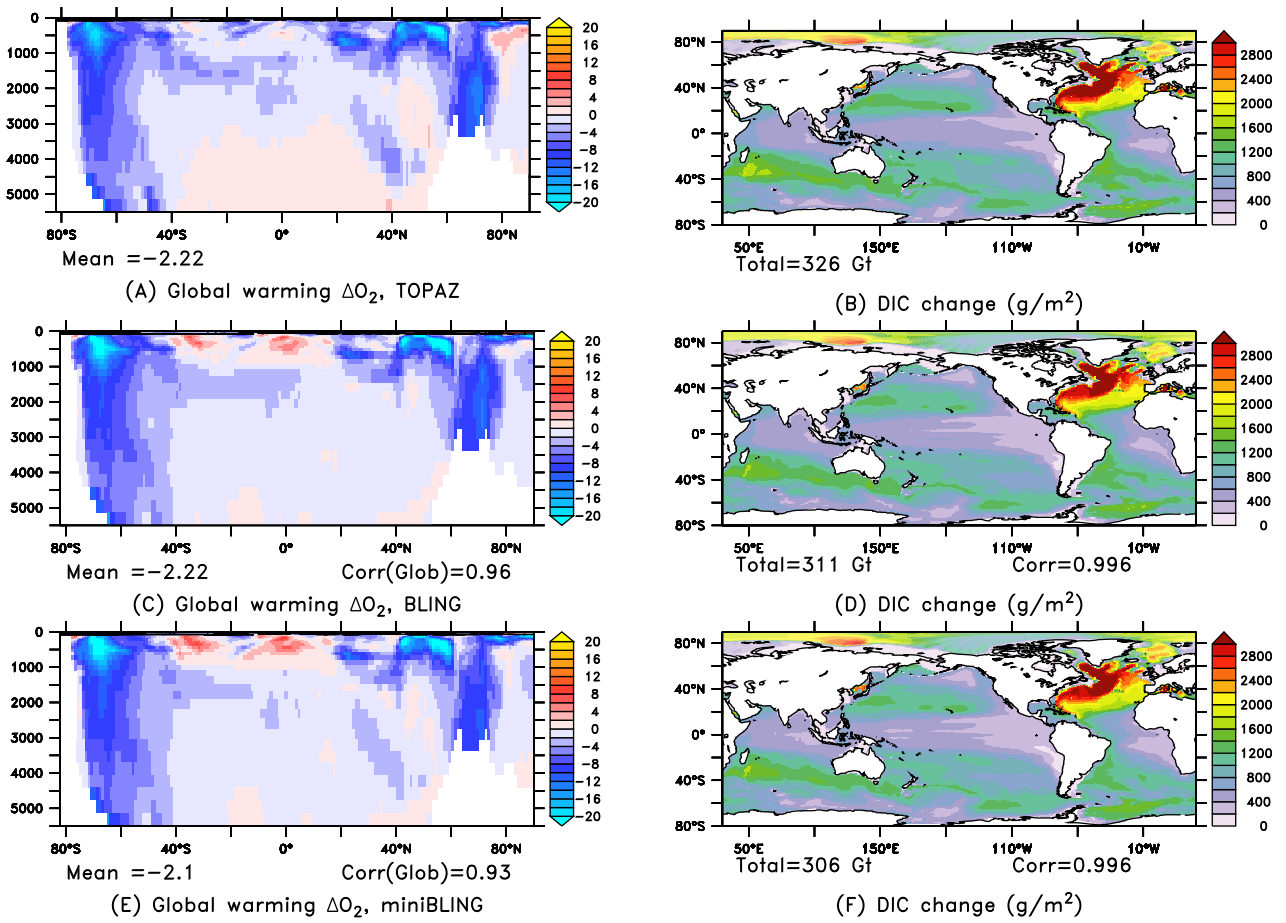

Figure 11. Changes in oxygen and DIC with CO_2 increase. Changes in oxygen are zonal means, given in μM, while changes in DIC are vertical integrals. Correlation coefficients are for BLING and miniBLING versus TOPAZ.

whole ocean to accumulate alkalinity, so that the average concentration rises by a little more than 1 μM. In the BLING model, rising CO_2 causes sinking calcium carbonate to dissolve more rapidly due to ocean acidification, which also increases surface alkalinity. However, the fact that carbonate production in BLING does not depend on the carbonate saturation state, perhaps coupled with the fact that changes in aragonite cycling are not resolved, causes the surface alkalinity increase to be less than in TOPAZ. This discrepancy could be largely resolved by adding a sensitivity of calcification to saturation state, as well as implicit aragonite cycling, to BLING, neither of which would require additional tracers. In the miniBLING model, alkalinity is pegged to salinity, and therefore does not increase at all over the simulation, as it does in the other two simulations, giving miniBLING the smallest carbon uptake.

4. Conclusions

We have demonstrated that highly parameterized ocean biogeochemical models with few tracers are capable of simulating a number of processes of great interest to the oceanography community. When run within the same physical circulation, both BLING and miniBLING produce spatial patterns of nutrients and oxygen that are comparable to those produced by the much more resource-intensive TOPAZ. The two computationally cheaper models also match the uptake of anthropogenic carbon within about 6%, with most of the discrepancy attributable to differences in ocean-acidification feedbacks on alkalinity cycling, which could be addressed with relatively minor effort. The pattern of global warming-induced changes in oxygen are also very similar across the models, suggesting that in this aspect at least, the simplified models are no worse at capturing the relevant dynamics of biological carbon storage than the more complex model.

A deeper examination shows that the models produce similar chemical changes in spite of significant differences in organic matter cycling. At high latitudes, BLING and miniBLING tend to produce much more export than TOPAZ during very strong, early blooms, while at low latitudes BLING and miniBLING produce insufficient export due to the relatively slow growth under these conditions, leading to unrealistically high nutrient concentrations. Nonetheless, it is likely that both of these shortcomings of the BLING models could be addressed with relatively minor changes to phytoplankton growth parameters and the remineralization profile, and by replacing the balanced growth assumption with a diagnostic (nonadvected) biomass tracer, none of which would significantly increase the computational cost. One clear drawback of the miniBLING design used here was the lack of a dissolved iron tracer. The degree to which the decoupling of iron and macronutrient cycling affected the results, particularly the tropical export bands, was unanticipated. Our recommendation, based on this experience, would be to include a prognostic iron tracer in any similar undertaking.

Our results can be viewed within the context of the field as it has progressed over the last three decades from the first coarse global biogeochemical models [*Maier-Reimer*, 1993] to the newest generation of high-resolution ocean eddying models with biogeochemistry e.g., *Duteil et al*. [2014]. A number of papers during this progression, such as *Matear and Holloway* [1995]; *Dietze and Loeptien* [2013], have emphasized the degree to which biogeochemical biases are artifacts of biases in the physical circulations. The three biogeochemical models used here are more sophisticated in their design than those of the earliest generation in use in the 1990s, including features such as iron-light colimitation and variable export fractions, which probably contributes to their improved skill. But the central role of physical processes in determining large-scale biogeochemical patterns through ocean circulation clearly emerges from the similarity of the three models in both their preindustrial and climate-warming simulations. Although our interests are scientific, it is our hope that this work will inform decision making about optimization of resources (physical resolution versus biogeochemical tracer number) in moving forward to high resolution simulations with ocean biogeochemistry.

One should also bear in mind that while treating the ecosystem through parameterizations may work reasonably well for large-scale biogeochemical cycling, there are potential pitfalls. As we have shown, the loss of mechanistic representation, inherent in simplified ecosystem parameterizations, could lead to unintended results in ways that are difficult to foresee. Thus, one must tread with caution during the development of models with few tracers, informed by insights gained from comprehensive, mechanistic models. The great promise of small tracer numbers lies in a more routine inclusion of realistic biogeochemical processes in high-resolution simulations.

Acknowledgments
Computational resources were provided to E.D.G by the Canadian Foundation for Innovation and Compute Canada. C.O.D. was supported by the National Aeronautics and Space Administration (NASA) under Award NNX14AL40G. K.B.R. was supported by the U.S. Department of Energy under Contract No. DE-SC0006848. The ESM2M code is available from the Modular Ocean Model development lab, which can be accessed at http://www.mom-ocean.org. The model runscript can be obtained from E.D.G. The miniBLING code is provided as supporting information. We thank Charles Stock for providing thoughtful comments on the manuscript. This work was sponsored by NSF's Southern Ocean Carbon and Climate Observations and Modeling (SOCCOM) Project under the NSF Award PLR-1425989.

References

Armstrong, R. A., C. Lee, J. I. Hedges, S. Honjo, and S. G. Wakeham (2001), A new, mechanistic model for organic carbon fluxes in the ocean based on the quantitative association of poc with ballast minerals, *Deep Sea Res., Part II*, *49*(1), 219–236.

Bacastow, R., and E. Maier-Reimer (1990), Ocean-circulation model of the carbon cycle, *Clim. Dyn.*, *4*, 95–125.

Beninca, E., J. Huisman, R. Heerkloss, K. D. Johnk, P. Branco, E. H. Van Nes, M. Scheffer, and S. P. Ellner (2008), Chaos in a long-term experiment with a plankton community, *Nature*, *451*(7180), 822–825, doi:10.1038/nature06512.

Bernardello, R., I. Marinov, J. B. Palter, J. L. Sarmiento, E. D. Galbraith, and R. D. Slater (2013), Response of the ocean natural carbon storage to projected 21st century climate change, *J. Clim.*, *27*, 2033–2053.

Bianchi, D., J. P. Dunne, J. L. Sarmiento, and E. D. Galbraith (2012), Data-based estimates of suboxia, denitrification, and N_2O production in the ocean and their sensitivities to dissolved O_2, *Global Biogeochem. Cycles*, *26*, GB2009, doi:10.1029/2011GB004209.

Bopp, L., P. Monfray, O. Aumont, J. L. Dufresne, H. Le Treut, G. Madec, L. Terray, and J. C. Orr (2001), Potential impact of climate change on marine export production, *Global Biogeochem. Cycles*, *15*(1), 81–99.

Bopp, L., L. Resplandy, J. Orr, S. Doney, J. Dunne, M. Gehlen, P. Halloran, C. Heinze, T. Ilyina, and R. Séférian (2013), Multiple stressors of ocean ecosystems in the 21st century: Projections with CMIP5 models, *Biogeosciences*, *10*(10), 6225–6245.

Cheung, W. W., V. W. Lam, J. L. Sarmiento, K. Kearney, R. Watson, D. Zeller, and D. Pauly (2010), Large-scale redistribution of maximum fisheries catch potential in the global ocean under climate change, *Global Change Biol.*, *16*(1), 24–35.

Christian, J. R. (2007), Advection in plankton models with variable elemental ratios, *Ocean Dyn.*, *57*(1), 63–71.

Dietze, H., and U. Loeptien (2013), Revisiting "nutrient trapping" in global coupled biogeochemical ocean circulation models, *Global Biogeochem. Cycles*, *27*, 265–284, doi:10.1002/gbc.20029.

Doney, S. C., V. J. Fabry, R. A. Feely, and J. A. Kleypas (2009), Ocean acidification: The other CO_2 problem, *Annu. Rev. Mar. Sci.*, *1*, 169192.

Dunne, J. P., R. A. Armstrong, A. Gnanadesikan, and J. L. Sarmiento (2005), Empirical and mechanistic models for the particle export ratio, *Global Biogeochem. Cycles*, *19*, GB4026, doi:10.1029/2004GB002390.

Dunne, J. P., J. L. Sarmiento, and A. Gnanadesikan (2007), A synthesis of global particle export from the surface ocean and cycling through the ocean interior and on the seafloor, *Global Biogeochem. Cycles*, *21*, GB4006, doi:10.1029/2006GB002907.

Dunne, J. P., et al. (2012), GFDL's ESM2 global coupled climate–carbon earth system models. Part I: Physical formulation and baseline simulation characteristics, *J. Clim.*, *25*(19), 6646–6665, doi:10.1175/jcli-d-11-00560.1.

Dunne, J. P., et al. (2013), GFDL's ESM2 global coupled climate–carbon earth system models. Part ii: Carbon system formulation and baseline simulation characteristics*, *J. Clim.*, *26*(7), 2247–2267.
Duteil, O., F. U. Schwarzkopf, C. W. Böning, and A. Oschlies (2014), Major role of the equatorial current system in setting oxygen levels in the eastern tropical Atlantic ocean: A high-resolution model study, *Geophys. Res. Lett.*, *41*, 2033–2040, doi:10.1002/2013GL058888.
Friedrichs, M. A. M., et al. (2007), Assessment of skill and portability in regional marine biogeochemical models: Role of multiple planktonic groups, *J. Geophys. Res.*, *112*, C08001, doi:10.1029/2006JC003852.
Frölicher, T., F. Joos, G.-K. Plattner, M. Steinacher, and S. C. Doney (2009), Natural variability and anthropogenic trends in oceanic oxygen in a coupled carbon cycle–climate model ensemble, *Global Biogeochem. Cycles*, *23*, GB1003, *doi*:10.1029/2008GB003316.
Galbraith, E. D., A. Gnanadesikan, J. P. Dunne, and M. R. Hiscock (2010), Regional impacts of iron-light colimitation in a global biogeochemical model, *Biogeosciences*, *7*(3), 1043–1064.
Garcia, H. E., R. Locarnini, T. P. Boyer, J. I. Antonov, M. Baranova, J. Zweng, and D. Johnson (2014a), *Dissolved Inorganic Nutrients Phosphate, Nitrate, Silicate*, *World Ocean Atlas 2013*, vol. 4, National Oceanic and Atmospheric Administration (NOAA).
Garcia, H. E., R. Locarnini, T. P. Boyer, J. I. Antonov, M. Baranova, J. Zweng, and D. Johnson (2014b), *Dissolved Oxygen, Apparent Oxygen Utilization, and Oxygen Saturation, World Ocean Atlas 2013*, vol. 4, NOAA.
Gnanadesikan, A., D. Bianchi, and M.-A. Pradal (2013), Critical role for mesoscale eddy diffusion in supplying oxygen to hypoxic ocean waters, *Geophys. Res. Lett.*, *40*, 5194–5198, doi:10.1002/grl.50998.
Gnanadesikan, A., J. Dunne, and R. Msadek (2014), Connecting Atlantic temperature variability and biological cycling in two earth system models, *J. Mar. Syst.*, *133*, 39–54.
Gruber, N., C. Hauri, Z. Lachkar, D. Loher, T. L. Frölicher, and G.-K. Plattner (2012), Rapid progression of ocean acidification in the California Current System, *Science*, *337*(6091), 220–223.
Key, R. M., A. Kozyr, C. L. Sabine, K. Lee, R. Wanninkhof, J. L. Bullister, R. A. Feely, F. J. Millero, C. Mordy, and T. H. Peng (2004), A global ocean carbon climatology: Results from Global Data Analysis Project (GLODAP), *Global Biogeochem. Cycles*, *18*, GB4031, doi:10.1029/2004GB002247.
Klaas, C., and D. E. Archer (2002), Association of sinking organic matter with various types of mineral ballast in the deep sea: Implications for the rain ratio, *Global Biogeochem. Cycles*, *16*(4), 1116, doi:10.1029/2001GB001765.
Kriest, I., S. Khatiwala, and A. Oschlies (2010), Towards an assessment of simple global marine biogeochemical models of different complexity, *Prog. Oceanogr.*, *86*, 337–360.
Kroeker, K. J., R. L. Kordas, R. Crim, I. E. Hendriks, L. Ramajo, G. S. Singh, C. M. Duarte, and J.-P. Gattuso (2013), Impacts of ocean acidification on marine organisms: Quantifying sensitivities and interaction with warming, *Global Change Biol.*, *19*(6), 1884–1896.
Kwiatkowski, L., et al. (2014), Imarnet: An ocean biogeochemistry model intercomparison project within a common physical ocean modelling framework, *Biogeosciences*, *11*(24), 7291–7304, doi:10.5194/bg-11-7291-2014.
Mahadevan, A., E. D'Asaro, C. Lee, and M. J. Perry (2012), Eddy-driven stratification initiates north Atlantic spring phytoplankton blooms, *Science*, *337*(6090), 54–58, doi:10.1126/science.1218740.
Maier-Reimer, E. (1993), Geochemical cycles in an ocean general circulation model. Preindustrial tracer distributions, *Global Biogeochem. Cycles*, *7*(3), 645–677.
Marinov, I., M. Follows, A. Gnanadesikan, J. L. Sarmiento, and R. D. Slater (2008), How does ocean biology affect atmospheric pco_2? Theory and models, *J. Geophys. Res.*, *113*, *C07032*, doi:10.1029/2007JC004598.
Marsay, C. M., R. J. Sanders, S. A. Henson, K. Pabortsava, E. P. Achterberg, and R. S. Lampitt (2015), Attenuation of sinking particulate organic carbon flux through the mesopelagic ocean, *Proc. Natl. Acad. Sci. U. S. A.*, *112*(4), 1089–1094, doi:10.1073/pnas.1415311112.
Matear, R., and A. Hirst (2003), Long-term changes in dissolved oxygen concentrations in the ocean caused by protracted global warming, *Global Biogeochem. Cycles*, *17*(4), 1125, doi:10.1029/2002GB001997.
Matear, R. J., and G. Holloway (1995), Modeling the inorganic phosphorus cycle of the north pacific using an adjoint data assimilation model to assess the role of dissolved organic phosphorus, *Global Biogeochem. Cycles*, *9*(1), 101–119.
Moore, C. M., et al. (2013), Processes and patterns of oceanic nutrient limitation, *Nat. Geosci.*, 701–710, doi:10.1038/ngeo1765.
Orr, J. C., et al. (2005), Anthropogenic ocean acidification over the twenty-first century and its impact on calcifying organisms, *Nature*, *437*(7059), 681–686.
Oschlies, A., and V. Garçon (1999), An eddy?permitting coupled physical?biological model of the North Atlantic: 1. Sensitivity to advection numerics and mixed layer physics, *Global Biogeochem. Cycles*, *13*(1), 135–160.
Sarmiento, J. L., R. D. Slater, M. Fasham, H. W. Ducklow, J. R. Toggweiler, and G. T. Evans (1993), A seasonal three-dimensional ecosystem model of nitrogen cycling in the north Atlantic euphotic zone, *Global Biochem. Cycles*, *7*(2), 417–450.
Schmittner, A., A. Oschlies, H. D. Matthews, and E. D. Galbraith (2008), Future changes in climate, ocean circulation, ecosystems, and biogeochemical cycling simulated for a business-as-usual CO_2 emission scenario until year 4000 AD, *Global Biogeochem. Cycles*, *22*, GB1013, doi:10.1029/2007GB002953.
Séférian, R., L. Bopp, M. Gehlen, J. C. Orr, C. Ethé, P. Cadule, O. Aumont, D. S. y Mélia, A. Voldoire, and G. Madec (2013), Skill assessment of three earth system models with common marine biogeochemistry, *Clim. Dyn.*, *40*(9–10), 2549–2573.
Siegenthaler, U., and J. Sarmiento (1993), Atmospheric carbon dioxide and the ocean, *Nature*, *365*(6442), 119–125.
Sigman, D. M., and E. A. Boyle (2000), Glacial/interglacial variations in atmospheric carbon dioxide, *Nature*, *407*(6806), 859–869.
Sinha, B., E. T. Buitenhuis, C. Le Quéré, and T. R. Anderson (2010), Comparison of the emergent behavior of a complex ecosystem model in two ocean general circulation models, *Prog. Oceanogr.*, *84*(3), 204–224.
Steinacher, M., et al. (2010), Projected 21st century decrease in marine productivity: A multi-model analysis, *Biogeosciences*, *7*(3), 979–1005.
Stommel, H. (1979), Determination of watermass properties of water pumped down from the Ekman layer to the geostrophic flow below, *Proc. Natl. Acad. Sci. U. S. A.*, *76*(7), 3051–3055.
Wanninkhof, R., et al. (2013), Global ocean carbon uptake: Magnitude, variability and trends, *Biogeosciences*, *10*, 1983–2000.
Ward, B. A., M. A. Friedrichs, T. R. Anderson, and A. Oschlies (2010), Parameter optimisation techniques and the problem of underdetermination in marine biogeochemical models, *J. Mar. Syst.*, *81*(1), 34–43.